
**COVER PAGE**

***Document downloaded by @DAEL***

***Wed May 27 17:11:24 2026***

***For personal use***

When automatic English translation is provided, only the original document is authentic.

The EAA cannot be held responsible of any translation error

Bibliographical reference

*A Numerical MFS Model for Computational Analysis of Acoustic Horns*, L. Godinho, P. Amado Mendes, J. Ramis, W. Cardenas and J. Carbajo, Acta Acustica **vol. 98** (Number 6), 2012, pp. 916-927

DOI

https://doi.org/10.3813/AAA.918575

**Acta Acustica united with Acustica**
**Vol. 98 (2012) 916 – 927**

DOI 10.3813/AAA.918575

# A Numerical MFS Model for Computational Analysis of Acoustic Horns

L. Godinho[1)], P. Amado Mendes[1)], J. Ramis[2)], W. Cardenas[2)], J. Carbajo[2)]

[1)] CICC, Department of Civil Engineering, Pólo 2 – FCTUC, Rua Luís Reis Santos, 3030-788 Coimbra, Portugal. lgodinho@dec.uc.pt

[2)] Department of Physics, System Engineering and Signal Theory, Mail Box 99, 03080 Alicante, Spain

**Summary**

This paper presents a numerical model based on the Method of Fundamental Solutions (MFS) for the computational analysis of acoustic horns. The model is here presented in detail for 2D and axisymmetric problems, and it is based on the use of two sub-regions, one of them containing the acoustic horn itself, and the other simulating a semi-infinite space with perfectly reflecting boundary. The proposed model is tested against well established methodologies, such as the BEM and the FEM, and it is shown to provide accurate results. Besides its numerical verification, application examples concerning the evaluation of horn directivity are shown, including non-trivial geometrical configurations. Comparison with experimental measurements of the horn directivity at different frequencies reveals a very good match between theoretical and laboratorial results, and thus indicates that the proposed approach can be an interesting tool in the analysis of acoustic horns.

**PACS no. 43.38.Ja**

## 1. Introduction

Acoustic horns are interface devices connected to the front face of a direct or indirect radiation loudspeaker. They play two important roles in acoustics systems. Firstly, they are used as directional control devices since they allow guiding the airborne acoustic energy into particular directions, thus they might be considered waveguides. Secondly, horns act as impedance matching devices, similar to the electrical transformers, increasing radiating system's efficiency [1].

The fundamentals of acoustic horns were widely developed by Euler, Lord Rayleigh and Webster. Webster was the first to introduce the concepts of specific acoustic impedance and the analogous acoustic impedance, both extensively used concepts in acoustics analysis. This author established what is known as Webster's horn equation, and its applicability was discussed by Putland in [2], concluding that indeed it governs acoustic propagation if the pressure field can be defined as a function of a single geometric parameter; however, these fields are restricted to those cases in which the level surfaces correspond to planes, concentric cylinders and spheres. It is worth mentioning that, in spite of the nowadays acceptance of the name "Webster's horn equation", Eisner [3], in his excellent review paper, cited mainly Bernoulli and Lagrange for the derivation of the horn equation, claiming that most of the mathematical treatments and derivations were known more than 150 years before Webster's work.

Based on the works carried out by Webster (1919) and Salmon (1946), the audio engineering community has designed different types of horns analyzing their cut-off frequency and proper size. D. Keele [4] has developed a frequency dependent constant directivity device, achieved by joining an exponential or hyperbolic throat segment, for driver loading, with two conical mouth segments, for directivity control.

At present, according to the need to design horn systems capable of improving efficiency and directional characteristics, a variety of numerical methods have been applied to simulate and optimize different types of geometries and configurations. Among those methodologies, the three most widely employed numerical techniques are the Boundary Element Method (BEM), the Finite Difference Method (FDM) and the Finite Element Method (FEM).

Morita *et al.* [5] and Beltran [6] used the Finite Element Analysis (FEA) to model axisymmetric horns. Within the analysis, Morita *et al.* used a radiation boundary condition, corresponding to an analytical integral equation defined over the mouth of the horn, that assumes that the horn is mounted in an infinite baffle. This approach reduced the numerical complexity of the system, taking into account the effect of the variation of the acoustic particle velocity across the mouth of the horn being modelled. Beltran used a non-reflective boundary condition on a spherical surface around the horn's mouth, requiring meshing the outside region in front of the horn. He also modeled the mechano-acoustic interaction of the compression driver diaphragm

Received 14 March 2012,
accepted 26 August 2012.



© S. Hirzel Verlag · EAA

*Document downloaded by @DAEL, 2026-05-27 17:11:28 - personal use only*

coupled to the horn throat, for different material properties, showing the usefulness and advantages of a FEA approach to the design of the complete radiating system.

Hodgson and Underwood [7] used a BEM scheme to compute the throat impedance and the far field pressure, demonstrating good agreement with experimental data; they also analyzed the correlation between the impedance peaks and the far field pressure response peaks. Noreland *et al.* [8] and Udawalpola *et al.* [9] applied a gradient-based optimization algorithm to improve the transmission properties of a variable mouth acoustic horn, by computing the reflection spectra using FEM and BEM methodologies. These authors remarked the advantages of using a BEM model, since it is not necessary to remesh or modify the volume mesh within the optimization processes. In the other hand, Makarski [10] proposed a computational tool based on the BEM and modal decomposition, with its focus on the professional development of horn loudspeakers, in which the electroacoustic transducer and the horn are treated separately.

Morgans [11] describes an optimization method, applied using FEM, BEM and a BEM variant (named Source-Superposition technique), for the design of constant beamwidth horn loaded loudspeakers. Using the Transmission Matrix Method, Lampton [12] and Patrick [13] established a numerical approach, which consists of discretizing complex geometry of electroacoustic systems using small cascade-elements network. Each acoustic component can be described by a pair of pressure and volume velocity ports at the input and output of the element, being these related by a 2x2 matrix. Adopting the Transmission Matrix approach, McLean *et al.* [14] studied the throat impedance characteristics of constant directivity horns, showing a good agreement between experimental and computed results.

Mostly in the last decade, a different class of numerical methods has been progressively developed. Those methods are usually so called meshless methods, as they require neither domain nor boundary discretization. Many techniques can be incorporated in this group, such as the MLPG-Meshless-Local-Petrov-Galerkin [15], Kansa's Method [16, 17] or the Method of Fundamental Solutions (MFS).The latter technique is, in fact, a boundary-only technique, in which the pressure field within a given domain is obtained using a linear combination of the effects of virtual sources located outside this domain. In this process, boundary conditions are enforced only at a limited number of boundary points, giving rise to a linear system of equations whose unknowns are the amplitudes of the virtual sources. As in the BEM, the MFS also requires the prior knowledge of the fundamental solutions, but its mathematical formulation and computational implementation are considerably simpler. Reference papers by Fairweather and Karageorghis [18], Fairweather *et al.* [19] and Golberg and Chen [20] describe the MFS and some of its possible applications.

It is important to note that, despite the simple conceptual basis of the method, many of the published works dealing with the MFS indicate that it can provide very accurate solutions to different types of physical problems, including those related to acoustics and wave propagation, to the case of heat and mass transfer or to the structural behaviour of solid structures. When compared with classical techniques, such as the FEM and the FDM, one can easily understand that it can be very efficient, namely because the MFS only requires the definition of discrete points along the boundaries, while the FEM or the FDM require a complete discretization of the domain to allow a solution to be obtained; from this point of view, the MFS can be seen as an interesting analysis tool. Although the more classical BEM also requires only boundary discretization, it should be noted that the formulation of the MFS does not require any integrations along the boundary (the BEM requires the evaluation of singular or even hyper-singular integrals), and thus it can also be more efficient than the BEM from a computational point of view. It may also be mentioned that the source-superposition technique used by Morgans [11], which uses a discretization scheme similar to the BEM and then computes the solution combining the effects of monopoles and dipoles centred on each boundary element, has some similarities with the MFS. However, that technique still requires a more intricate mathematical treatment, including the calculation of surface integrals.

Although different studies have been published on the use of the technique in acoustics, they are mostly restricted to solving the Helmholtz equation in problems involving two-dimensional domains. Alves and Valtchev [21] compared the plane waves method and the MFS for acoustic wave scattering. Godinho *et al.* [22] studied the accuracy of the MFS in the analysis of 2D acoustic and heat transfer problems, concluding that the method is very accurate for the study of smooth geometrical configurations. Later, the same authors (Godinho *et al.* [23]) implemented the MFS together with domain decomposition techniques to simulate wave propagation around thin elements and cracks. Little is published concerning the MFS application to either axisymmetric or 3D acoustic problems, in particular concerning more complex problems with connected subdomains. António *et al.* [24] simulated the sound propagation within a closed space, using a MFS formulation. In that work, the authors used a single-domain formulation, and concluded that the accuracy of the method depends on the number and location of the virtual sources. Very recently, Godinho *et al.* [25] also addressed the 3D evaluation of the pressure field in two 3D enclosures connected by an opening using the MFS, describing the geometry by means of two coupled subdomains. Interestingly, to the authors' knowledge the application of the MFS to the study of axisymmetric engineering problems has not yet been reported in the literature.

The purpose of this work is thus to present an efficient and accurate numerical model to solve problems related with acoustic horn analysis considering 2D and axisymmetric geometries using the Method of Fundamental Solutions. The proposed model can be seen as a different approach when compared with existing published works,



Document downloaded by @DAEL, 2026-05-27 17:11:28 - personal use only

with fundamental advantages related to its meshing simplicity and lower computational cost.

The structure of this paper is as follows: in section 2 the mathematical formulation of the governing equations in sound propagation is briefly outlined, indicating the fundamental solutions for pressure and particle velocity (both for the 2D, 3D and axisymmetric cases), and formulating the Method of Fundamental Solutions (MFS) in the frequency domain, for simple and multiple subdomains; in section 3, a MFS model is described for the analysis of a radiating acoustic horn embedded in a rigid infinite screen; section 4 presents a verification of the MFS model, by comparing an important transmission characteristic of the acoustic horns, the throat impedance, for 2D and axisymmetric configurations against reference BEM and FEM results; in section 5, a comparison of the sound directivity computed using the MFS and the FEM for two horn configurations is presented; finally, section 6 addresses the main conclusions of this paper.

## 2. General mathematical formulation

### 2.1. Governing equations

The propagation of sound within a homogeneous acoustic space can be mathematically represented in the frequency domain by the Helmholtz differential equation,

$$\nabla^2 p + k^2 p = 0, \tag{1}$$

where

$$\nabla^2 = \frac{\partial^2}{\partial x^2} + \frac{\partial^2}{\partial y^2} + \frac{\partial^2}{\partial z^2}$$

in the case of a 3D problem, and

$$\nabla^2 = \frac{\partial^2}{\partial x^2} + \frac{\partial^2}{\partial y^2}$$

for the 2D case; $p$ is the acoustic pressure, $k = \omega/c$ the wave number, $\omega = 2\pi f$ the angular frequency, $f$ the frequency and $c$ the sound propagation velocity within the acoustic medium.

### 2.2. Fundamental solutions

For the 3D case, assuming a point source placed within the propagation domain, at point $\boldsymbol{x}_0$ with coordinates $(x_0, y_0, z_0)$, it is possible to establish fundamental solutions, $G$ for the sound pressure and $H$ for the particle velocity at a point $\boldsymbol{x}$ with coordinates $(x, y, z)$, which can be written respectively as

$$G^{3D}(\boldsymbol{x}, \boldsymbol{x}_0, k) = \frac{1}{r} e^{-ikr}, \tag{2}$$

$$H^{3D}(\boldsymbol{x}, \boldsymbol{x}_0, k, \vec{n}) = \frac{1}{-i\rho\omega} \frac{-ikr - 1}{r^2} e^{-ikr} \frac{\partial r}{\partial \vec{n}}. \tag{3}$$

If a 2D configuration is analyzed, assuming a line source placed within this propagation domain, at point $\boldsymbol{x}_0$ with coordinates $(x_0, y_0)$, the corresponding fundamental solutions become

$$G^{2D}(\boldsymbol{x}, \boldsymbol{x}_0, k) = -\frac{i}{4} H_0^{(2)}(kr), \tag{4}$$

$$H^{2D}(\boldsymbol{x}, \boldsymbol{x}_0, k, \vec{n}) = \frac{k}{-4\rho\omega} H_1^{(2)}(kr) \frac{\partial r}{\partial \vec{n}}. \tag{5}$$

For both cases, $r$ corresponds to the distance between the source point and the domain point, given in 3D by $r = \sqrt{(x-x_0)^2 + (y-y_0)^2 + (z-z_0)^2}$ and in 2D by $r = \sqrt{(x-x_0)^2 + (y-y_0)^2}$; $\vec{n}$ represents the direction along which the particle velocity is calculated and $\rho$ the medium density.

A special case can be considered when an axisymmetric problem is analyzed, for which it is also possible to establish a fundamental solution. For that case, assuming that the source is also axisymmetric (e.g. a circular ring) and with its centre over the $x$ axis, the required fundamental solutions become

$$G^{Axi}(\boldsymbol{x}, \boldsymbol{x}_0, k) = \int_0^{2\pi} \frac{1}{r(\theta)} e^{-ikr(\theta)} d\theta, \tag{6}$$

$$H^{Axi}(\boldsymbol{x}, \boldsymbol{x}_0, k, \vec{n}) = \frac{1}{-i\rho\omega} \int_0^{2\pi} \frac{-ikr(\theta) - 1}{r^2(\theta)} \cdot e^{-ikr(\theta)} \frac{\partial r(\theta)}{\partial \vec{n}} d\theta. \tag{7}$$

Equations (6) and (7) correspond, in practice, to the integration of a 3D source, given by equations (2) and (3), along the circle centred on the $x$ axis and passing through $(x_0, y_0, 0)$, being

$$r(\theta) = \sqrt{y^2 + y_0^2 - 2yy_0 \cos\theta + (x-x_0)^2}.$$

Therefore, it becomes obvious that if $(x_0, y_0, 0)$, and $(x, y, 0)$ coincide, then $r(0) = 0$, and hence a singularity occurs in the integrands of equations (6) and (7). However, if the source and receiver points are apart, then those integrals become non-singular, and can be easily approximated using standard numerical integration techniques.

All the above mentioned solutions can be extended to allow accounting for the presence of rigid vertical or horizontal planes by means of the image-source method. Considering the 2D problem, if an infinite rigid plane is located at $x = 0$ or at $y = 0$ (e.g. a symmetric problem with respect to $x = 0$ or to $y = 0$), the pressure field can be computed as

$$G^{2D}_{sym}(\boldsymbol{x}, \boldsymbol{x}_0, k) = -\frac{i}{4} H_0^{(2)}(kr) - \frac{i}{4} H_0^{(2)}(kr_1), \tag{8}$$

with $r_1 = \sqrt{(x \pm x_0)^2 + (y \mp y_0)^2}$ (where the sign of the first and second terms of the square root depend on whether symmetry is considered with respect to $x = 0$ or to $y = 0$).

Additionally, if a horizontal rigid plane is considered at $y = 0$, then the fundamental solution becomes

$$G^{2D}_{quater}(\boldsymbol{x}, \boldsymbol{x}_0, k) = -\frac{i}{4} H_0^{(2)}(kr) - \sum_{j=1}^{3} \frac{i}{4} H_0^{(2)}(kr_j), \tag{9}$$



Document downloaded by @DAEL, 2026-05-27 17:11:28 - personal use only

with

$$r_1 = \sqrt{(x+x_0)^2+(y-y_0)^2},$$
$$r_2 = \sqrt{(x+x_0)^2+(y+y_0)^2},$$
$$r_3 = \sqrt{(x-x_0)^2+(y+y_0)^2}.$$

Similarly, the concept of image-sources can be applied to 3D and axisymmetric problems. Since the present paper deals mostly with the latter, it is important to define the corresponding solution. Considering, for that case, a rigid vertical plane located at $x = 0$, the fundamental solution can be written as

$$G^{\mathrm{Axi}}_{\mathrm{sym}}(\boldsymbol{x}, \boldsymbol{x}_0, k) = \int_0^{2\pi} \left( \frac{\mathrm{e}^{-\mathrm{i}kr(\theta)}}{r(\theta)} + \frac{\mathrm{e}^{-\mathrm{i}kr_1(\theta)}}{r_1(\theta)} \right) \mathrm{d}\theta, \tag{10}$$

where $r_1(\theta) = \sqrt{y^2 + y_0^2 - 2yy_0\cos\theta + (x+x_0)^2}$.

### 2.3. The Method of Fundamental Solutions (MFS)

The MFS is a boundary method, in which the solution is approximated as a linear combination of the relevant fundamental solutions of the analysed problem. To formulate the method, consider a generic problem governed by equation (1), with a boundary $\Gamma = \Gamma_1 \cup \Gamma_2$ subject to Dirichlet (in $\Gamma_1$) and Neumann (in $\Gamma_2$) boundary conditions

$$p = p_K, \quad \text{in } \Gamma_1, \tag{11}$$
$$-\frac{1}{\mathrm{i}\rho\omega}\frac{\partial}{\partial \vec{n}} p = v_K, \quad \text{in } \Gamma_2, \tag{12}$$

where $\vec{n}$ represents the normal direction to the boundary.

To obtain a solution for this problem (either in 2D, 3D or axisymmetric conditions), it becomes necessary to simultaneously satisfy equations (1), (11) and (12), which usually is not a trivial task. However, the fundamental solutions presented previously automatically satisfy equation (1) for each specific type of problem, although they do not directly satisfy equations (11) and (12). Let us now consider a set of $NS$ source points distributed outside the analysis domain, and assume that the pressure field at a point $\boldsymbol{x}$ can be represented as a linear combination of the effects of the $NS$ sources positioned outside the domain, at $\boldsymbol{x}_j$, such that

$$p(\boldsymbol{x}, k) = \sum_{j=1}^{NS} Q_j G(\boldsymbol{x}, \boldsymbol{x_j}, k), \tag{13}$$

$Q_j$ being the unknown amplitude of each source.

For the described case, and given this representation, let us also define a set of $NC$ collocation points distributed along $\Gamma$. Forcing the required boundary conditions of equations (11) and (12) at each of the $NC$ collocation points, two sets of equations can now be written as

$$\sum_{j=1}^{NS} Q_j G(\boldsymbol{x}_i, \boldsymbol{x}_j, k) = p_{K,i} \quad \text{for each } \boldsymbol{x}_i \text{ in } \Gamma_1, \tag{14}$$

$$\sum_{j=1}^{NS} Q_j H(\boldsymbol{x}_i, \boldsymbol{x}_j, k, \vec{n}) = v_{K,i} \quad \text{for each } \boldsymbol{x}_i \text{ in } \Gamma_2, \tag{15}$$

with $p_{K,i}$ and $v_{K,i}$ being the prescribed pressure or velocities at collocation point $i$.

Establishing those equations, a system with $NC$ equations and $NS$ unknowns can be written and solved in order to obtain the $Q_j$ amplitudes. If $NS = NC$, then this system is a linear equation system, which can be solved using standard techniques. However, some published works (see for example [18]) suggest that the problem may also be transformed into a minimization problem, by using $NS < NC$. For that case, the functional

$$\sum_{i=1}^{NC1} \left( \overline{p}(\boldsymbol{x}_i, k) - p_{K,i} \right)^2 + \sum_{i=NC1+1}^{NC} \left( \overline{v}(\boldsymbol{x}_i, k, \vec{n}_i) - v_{K,i} \right)^2 \tag{16}$$

must be minimized, being $NC1$ the number of collocation points in $\Gamma_1$, $\overline{p}(\boldsymbol{x}_i, k)$ and $\overline{v}(\boldsymbol{x}_i, k, \vec{n}_i)$ the approximated solutions (in terms of pressure and normal velocity) at collocation point $i$. To perform this minimization, a least squares solver may be used. However, due to the good results obtained in previous works for 2D and 3D problems, we will not make use of this option in this paper.

### 2.4. MFS with multiple domains

The MFS formulation presented previously can be easily extended to allow the analysis of connected subdomains. An example of such application can be found in Godinho *et al.* [25] for the case of two interconnected 3D closed spaces. If we consider a system with two separate subdomains, $\Omega_1$ and $\Omega_2$, connected by an interface $\Gamma_c$, then the pressure field within the two sub-domains can be represented by two separate sets of virtual sources (with $NS1$ and $NS2$ sources, respectively), and can be written as

$$p(\boldsymbol{x}, k)_{\Omega_1} = \sum_{j=1}^{NS1} Q_j G(\boldsymbol{x}, \boldsymbol{x}_{1,j}, k) \quad \text{for } \boldsymbol{x} \text{ in } \Omega_1, \tag{17}$$

$$p(\boldsymbol{x}, k)_{\Omega_2} = \sum_{j=1}^{NS2} P_j G(\boldsymbol{x}, \boldsymbol{x}_{2,j}, k) \quad \text{for } \boldsymbol{x} \text{ in } \Omega_2. \tag{18}$$

Along the common boundary $\Gamma_c$, continuity conditions must be enforced, and can be written as

$$p(\boldsymbol{x}, k)_{\Omega_1} = p(\boldsymbol{x}, k)_{\Omega_2}, \tag{19}$$
$$v(\boldsymbol{x}, k, \vec{n})_{\Omega_1} = v(\boldsymbol{x}, k, \vec{n})_{\Omega_2}. \tag{20}$$

## 3. The MFS for the analysis of an emitting horn embedded in a rigid infinite screen

To apply the MFS to the analysis of an emitting horn, embedded within a rigid screen of infinite extent, consider the configuration schematically represented in Figure 1a. In that figure, at $x = L$ a rigid surface is considered, simulating an infinite rigid screen. To analyze this system using the MFS, a model with two sub-domains is considered, as described in Figure 1b, in which sub-domain $\Omega_1$ incorporates the geometry of the horn, while sub-domain $\Omega_2$ simulates the semi-infinite space and the rigid screen. The common interface, along which continuity of pressure and particle velocity must be imposed, is designated as $\Gamma_c$, while



Document downloaded by @DAEL, 2026-05-27 17:11:28 - personal use only

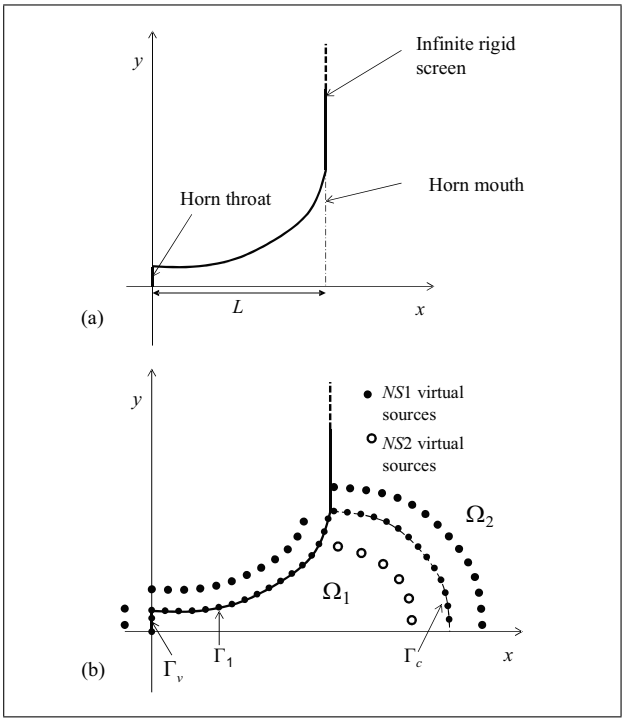


Figure 1. a) Schematic representation of the problem geometry; b) Distribution of virtual sources and collocation points in the MFS model with two sub-domains.

$\Gamma_1$ and $\Gamma_v$ correspond to surfaces along which the normal velocity is prescribed. To simulate the horn problem, null velocities are prescribed in $\Gamma_1$, while a unit velocity is prescribed in the vibrating surface $\Gamma_v$.

When a 2D geometry is to be analyzed, the problem can be stated considering that $y = 0$ is a symmetry axis, and thus the fundamental solutions defined in equations (8) and (9) can be used. For that purpose, for sub-domain $\Omega_1$ and considering that symmetry axis, the fundamental solution given by equation (8) is considered, and for subdomain $\Omega_2$ the Green's function given in equation (9) for a quarter space is considered in order to simulate the rigid screen. Thus, for this 2D case, the pressure field in both spaces will be defined by the equations

$$p(\boldsymbol{x}, k)_{\Omega_1} = \sum_{j=1}^{NS1} Q_j G^{\mathrm{2D}}_{\mathrm{sym}}(\boldsymbol{x}, \boldsymbol{x}_{1,j}, k) \quad \text{for } \boldsymbol{x} \text{ in } \Omega_1, \tag{21}$$

$$p(\boldsymbol{x}, k)_{\Omega_2} = \sum_{j=1}^{NS2} P_j G^{\mathrm{2D}}_{\mathrm{quater}}(\boldsymbol{x}, \boldsymbol{x}_{2,j}, k) \quad \text{for } \boldsymbol{x} \text{ in } \Omega_2. \tag{22}$$

To obtain the unknowns $Q_j$ and $P_j$ an equation system can be defined by imposing the relevant boundary conditions. So, in order to illustrate the implementation of the MFS for the analysis of the emitting horn represented in Figure 1, the construction of the equation system is now described. Therefore, consider $N_v$ points where a unit velocity is prescribed along the vibrating surface/boundary $\Gamma_v$ ($\overline{\boldsymbol{x}}_{i,\Gamma_v}$ being the $i$th point) and $N1$ points along the rigid boundary $\Gamma_1$ where a null velocity is enforced ($\overline{\boldsymbol{x}}_{i,\Gamma_1}$ being the $i$th point); moreover, a number $NBC$ of points ($\overline{\boldsymbol{x}}_{i,\Gamma_c}$ being the $i$th point) are used to define the common interface $\Gamma_c$ between sub-domains $\Omega_1$ and $\Omega_2$, and to impose continuity of pressure and particle velocity. Outside each subdomain, $NS1$ and $NS2$ virtual sources are used to define the correspondent sound fields ($\boldsymbol{x}_{i,j}$ being the $i$th source of subdomain $j$). For this case, the resulting equation system, in the presence of a vibrating boundary within sub-domain 1, can be defined as $Ax = B$ with

$$A = \begin{bmatrix}
H^{\mathrm{2D}}_{\mathrm{sym}}(\overline{\boldsymbol{x}}_{1,\Gamma_v}, \boldsymbol{x}_{1,1}, k, \vec{n}) & \cdots & H^{\mathrm{2D}}_{\mathrm{sym}}(\overline{\boldsymbol{x}}_{1,\Gamma_v}, \boldsymbol{x}_{NS1,1}, k, \vec{n}) \\
\vdots & & \vdots \\
H^{\mathrm{2D}}_{\mathrm{sym}}(\overline{\boldsymbol{x}}_{N_v,\Gamma_v}, \boldsymbol{x}_{1,1}, k, \vec{n}) & \cdots & H^{\mathrm{2D}}_{\mathrm{sym}}(\overline{\boldsymbol{x}}_{N_v,\Gamma_v}, \boldsymbol{x}_{NS1,1}, k, \vec{n}) \\
H^{\mathrm{2D}}_{\mathrm{sym}}(\overline{\boldsymbol{x}}_{1,\Gamma_1}, \boldsymbol{x}_{1,1}, k, \vec{n}) & \cdots & H^{\mathrm{2D}}_{\mathrm{sym}}(\overline{\boldsymbol{x}}_{1,\Gamma_1}, \boldsymbol{x}_{NS1,1}, k, \vec{n}) \\
\vdots & & \vdots \\
H^{\mathrm{2D}}_{\mathrm{sym}}(\overline{\boldsymbol{x}}_{N_1,\Gamma_1}, \boldsymbol{x}_{1,1}, k, \vec{n}) & \cdots & H^{\mathrm{2D}}_{\mathrm{sym}}(\overline{\boldsymbol{x}}_{N_1,\Gamma_1}, \boldsymbol{x}_{NS1,1}, k, \vec{n}) \\
H^{\mathrm{2D}}_{\mathrm{sym}}(\overline{\boldsymbol{x}}_{1,\Gamma_c}, \boldsymbol{x}_{1,1}, k, \vec{n}) & \cdots & H^{\mathrm{2D}}_{\mathrm{sym}}(\overline{\boldsymbol{x}}_{1,\Gamma_c}, \boldsymbol{x}_{NS1,1}, k, \vec{n}) \\
\vdots & & \vdots \\
H^{\mathrm{2D}}_{\mathrm{sym}}(\overline{\boldsymbol{x}}_{NBC,\Gamma_c}, \boldsymbol{x}_{1,1}, k, \vec{n}) & \cdots & H^{\mathrm{2D}}_{\mathrm{sym}}(\overline{\boldsymbol{x}}_{NBC,\Gamma_c}, \boldsymbol{x}_{NS1,1}, k, \vec{n}) \\
G^{\mathrm{2D}}_{\mathrm{sym}}(\overline{\boldsymbol{x}}_{1,\Gamma_c}, \boldsymbol{x}_{1,1}, k) & \cdots & G^{\mathrm{2D}}_{\mathrm{sym}}(\overline{\boldsymbol{x}}_{1,\Gamma_c}, \boldsymbol{x}_{NS1,1}, k) \\
\vdots & & \vdots \\
G^{\mathrm{2D}}_{\mathrm{sym}}(\overline{\boldsymbol{x}}_{NBC,\Gamma_c}, \boldsymbol{x}_{1,1}, k) & \cdots & G^{\mathrm{2D}}_{\mathrm{sym}}(\overline{\boldsymbol{x}}_{NBC,\Gamma_c}, \boldsymbol{x}_{NS1,1}, k)
\end{bmatrix}$$

$$\begin{bmatrix}
0 & \cdots \\
\vdots & \\
0 & \cdots \\
0 & \cdots \\
\vdots & \\
0 & \cdots \\
-H^{\mathrm{2D}}_{\mathrm{quarter}}(\overline{\boldsymbol{x}}_{1,\Gamma_c}, \boldsymbol{x}_{1,2}, k, \vec{n}) & \cdots \\
\vdots & \\
-H^{\mathrm{2D}}_{\mathrm{quarter}}(\overline{\boldsymbol{x}}_{NBC,\Gamma_v}, \boldsymbol{x}_{1,2}, k, \vec{n}) & \cdots \\
-G^{\mathrm{2D}}_{\mathrm{quarter}}(\overline{\boldsymbol{x}}_{1,\Gamma_c}, \boldsymbol{x}_{1,2}, k) & \cdots \\
\vdots & \\
-G^{\mathrm{2D}}_{\mathrm{quarter}}(\overline{\boldsymbol{x}}_{NBC,\Gamma_c}, \boldsymbol{x}_{1,2}, k) & \cdots
\end{bmatrix}$$

$$\begin{bmatrix}
\cdots & 0 \\
 & \vdots \\
\cdots & 0 \\
\cdots & 0 \\
 & \vdots \\
\cdots & 0 \\
\cdots & -H^{\mathrm{2D}}_{\mathrm{quarter}}(\overline{\boldsymbol{x}}_{1,\Gamma_c}, \boldsymbol{x}_{NS2,2}, k, \vec{n}) \\
 & \vdots \\
\cdots & -H^{\mathrm{2D}}_{\mathrm{quarter}}(\overline{\boldsymbol{x}}_{NBC,\Gamma_v}, \boldsymbol{x}_{NS2,2}, k, \vec{n}) \\
\cdots & -G^{\mathrm{2D}}_{\mathrm{quarter}}(\overline{\boldsymbol{x}}_{1,\Gamma_c}, \boldsymbol{x}_{NS2,2}, k) \\
 & \vdots \\
\cdots & -G^{\mathrm{2D}}_{\mathrm{quarter}}(\overline{\boldsymbol{x}}_{NBC,\Gamma_c}, \boldsymbol{x}_{NS2,2}, k)
\end{bmatrix},$$

$$x = \begin{bmatrix} Q_1 & \cdots & Q_{NS1} & P_1 & \cdots & P_{NS2} \end{bmatrix}^T,$$

$$B = \begin{bmatrix} 1 & \cdots & 1 & 0 & \cdots & 0 & 0 & \cdots & 0 & 0 & \cdots & 0 \end{bmatrix}^T. \tag{23}$$



*Document downloaded by @DAEL, 2026-05-27 17:11:28 - personal use only*

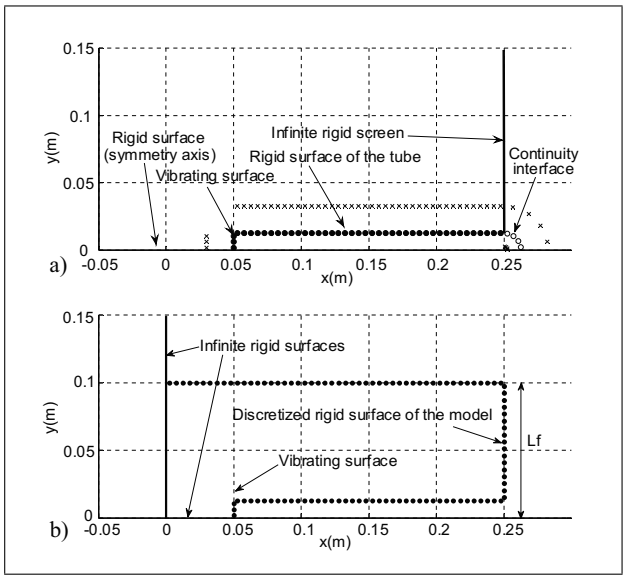


Figure 2. a) MFS model of the tube with one vibrating end and two connected subregions; b) Nodal points of the BEM model with a single region.

If an axisymmetric configuration is considered, the corresponding fundamental solutions to be used are those of equations (6) and (10), and the pressure field is then defined by

$$p(\boldsymbol{x},k)_{\Omega_1} = \sum_{j=1}^{NS1} Q_j G^{\mathrm{Axi}}(\boldsymbol{x},\boldsymbol{x}_{1,j},k) \quad \text{for } \boldsymbol{x} \text{ in } \Omega_1, \tag{24}$$

$$p(\boldsymbol{x},k)_{\Omega_2} = \sum_{j=1}^{NS2} P_j G^{\mathrm{Axi}}_{\mathrm{sym}}(\boldsymbol{x},\boldsymbol{x}_{2,j},k) \quad \text{for } \boldsymbol{x} \text{ in } \Omega_2. \tag{25}$$

In this axisymmetric case, the equation system $Ax = B$, needed to calculate the unknown amplitudes $Q_j$ and $P_j$, can be established by enforcing the appropriate boundary conditions in an analogous way to that illustrated in equation (23) and making use of the adequate fundamental solutions

$$A = \begin{bmatrix}
H^{\mathrm{Axi}}(\overline{\boldsymbol{x}}_{1,\Gamma_v},\boldsymbol{x}_{1,1},k,\vec{n}) & \cdots & H^{\mathrm{Axi}}(\overline{\boldsymbol{x}}_{1,\Gamma_v},\boldsymbol{x}_{NS1,1},k,\vec{n}) \\
\vdots & & \vdots \\
H^{\mathrm{Axi}}(\overline{\boldsymbol{x}}_{N_v,\Gamma_v},\boldsymbol{x}_{1,1},k,\vec{n}) & \cdots & H^{\mathrm{Axi}}(\overline{\boldsymbol{x}}_{N_v,\Gamma_v},\boldsymbol{x}_{NS1,1},k,\vec{n}) \\
H^{\mathrm{Axi}}(\overline{\boldsymbol{x}}_{1,\Gamma_1},\boldsymbol{x}_{1,1},k,\vec{n}) & \cdots & H^{\mathrm{Axi}}(\overline{\boldsymbol{x}}_{1,\Gamma_1},\boldsymbol{x}_{NS1,1},k,\vec{n}) \\
\vdots & & \vdots \\
H^{\mathrm{Axi}}(\overline{\boldsymbol{x}}_{N_1,\Gamma_1},\boldsymbol{x}_{1,1},k,\vec{n}) & \cdots & H^{\mathrm{Axi}}(\overline{\boldsymbol{x}}_{N_1,\Gamma_1},\boldsymbol{x}_{NS1,1},k,\vec{n}) \\
H^{\mathrm{Axi}}(\overline{\boldsymbol{x}}_{1,\Gamma_c},\boldsymbol{x}_{1,1},k,\vec{n}) & \cdots & H^{\mathrm{Axi}}(\overline{\boldsymbol{x}}_{1,\Gamma_c},\boldsymbol{x}_{NS1,1},k,\vec{n}) \\
\vdots & & \vdots \\
H^{\mathrm{Axi}}(\overline{\boldsymbol{x}}_{NBC,\Gamma_c},\boldsymbol{x}_{1,1},k,\vec{n}) & \cdots & H^{\mathrm{Axi}}(\overline{\boldsymbol{x}}_{NBC,\Gamma_c},\boldsymbol{x}_{NS1,1},k,\vec{n}) \\
G^{\mathrm{Axi}}(\overline{\boldsymbol{x}}_{1,\Gamma_c},\boldsymbol{x}_{1,1},k) & \cdots & G^{\mathrm{Axi}}(\overline{\boldsymbol{x}}_{1,\Gamma_c},\boldsymbol{x}_{NS1,1},k) \\
\vdots & & \vdots \\
G^{\mathrm{Axi}}(\overline{\boldsymbol{x}}_{NBC,\Gamma_c},\boldsymbol{x}_{1,1},k) & \cdots & G^{\mathrm{Axi}}(\overline{\boldsymbol{x}}_{NBC,\Gamma_c},\boldsymbol{x}_{NS1,1},k)
\end{bmatrix}$$

$$\begin{bmatrix}
0 & \cdots \\
\vdots & \\
0 & \cdots \\
0 & \cdots \\
\vdots & \\
0 & \cdots \\
-H^{\mathrm{Axi}}_{\mathrm{sym}}(\overline{\boldsymbol{x}}_{1,\Gamma_c},\boldsymbol{x}_{1,2},k,\vec{n}) & \cdots \\
\vdots & \\
-H^{\mathrm{Axi}}_{\mathrm{sym}}(\overline{\boldsymbol{x}}_{NBC,\Gamma_v},\boldsymbol{x}_{1,2},k,\vec{n}) & \cdots \\
-G^{\mathrm{Axi}}_{\mathrm{sym}}(\overline{\boldsymbol{x}}_{1,\Gamma_c},\boldsymbol{x}_{1,2},k) & \cdots \\
\vdots & \\
-G^{\mathrm{Axi}}_{\mathrm{sym}}(\overline{\boldsymbol{x}}_{NBC,\Gamma_c},\boldsymbol{x}_{1,2},k) & \cdots
\end{bmatrix}$$

$$\begin{bmatrix}
\cdots & 0 \\
 & \vdots \\
\cdots & 0 \\
\cdots & 0 \\
 & \vdots \\
\cdots & 0 \\
\cdots & -H^{\mathrm{Axi}}_{\mathrm{sym}}(\overline{\boldsymbol{x}}_{1,\Gamma_c},\boldsymbol{x}_{NS2,2},k,\vec{n}) \\
 & \vdots \\
\cdots & -H^{\mathrm{Axi}}_{\mathrm{sym}}(\overline{\boldsymbol{x}}_{NBC,\Gamma_c},\boldsymbol{x}_{NS2,2},k,\vec{n}) \\
\cdots & -G^{\mathrm{Axi}}_{\mathrm{sym}}(\overline{\boldsymbol{x}}_{1,\Gamma_c},\boldsymbol{x}_{NS2,2},k) \\
 & \vdots \\
\cdots & -G^{\mathrm{Axi}}_{\mathrm{sym}}(\overline{\boldsymbol{x}}_{NBC,\Gamma_c},\boldsymbol{x}_{NS2,2},k)
\end{bmatrix},$$

$$x = \begin{bmatrix} Q_1 & \cdots & Q_{NS1} & P_1 & \cdots & P_{NS2} \end{bmatrix}^T,$$

$$B = \begin{bmatrix} 1 & \cdots & 1 & 0 & \cdots & 0 & 0 & \cdots & 0 & 0 & \cdots & 0 \end{bmatrix}^T. \tag{26}$$

In the present paper, the authors only address the 2D and axially symmetric cases; it should be mentioned that other authors also proposed solution strategies for this type of problems, although adopting different methodologies such as in the papers by Pagneux *et al.* [26], Amir *et al.* [27] and Hélie [28]. It should also be stated that the extension of the method presented herein to full 3D problems should not pose significant difficulties, either from the mathematical or from the implementation points of view; previous works by António *et al.* [24] and Godinho *et al.* [25] indicate that the MFS may be applied in such cases with good results. This extension requires additional derivations of equations (2) and (3), but is beyond the scope of the present work. Additionally, as with other numerical methods, complex and large-scale 3D problems will increase significantly the needed computational resources.

## 4. Verification of the MFS model

To verify the correctness of the MFS algorithm, two sets of verifications will be performed. In the first set, the method is verified against a BEM solution for the 2D case; then, for the axisymmetric case, a comparison with commercial FEM software is performed.

To analyze the behaviour of the 2D MFS model, the system defined as depicted in Figure 2 is considered, in



*Document downloaded by @DAEL, 2026-05-27 17:11:28 - personal use only*

which a straight tube with one vibrating end is embedded within a rigid screen. For the presented case, the width of the tube is 0.0254 m, and its length is 0.2 m. Due to symmetry considerations, only half of the model needs to be discretized. Different discretizations and positions of the virtual sources have been tested for the MFS model (Figure 2a), and results were compared with those provided by a standard BEM model in which the maximum length of each boundary element was 0.005 m. It is worth noting that the BEM model made use of a single-domain region, and for that case the rigid screen was discretized in the vicinity of the tube opening using a flange length Lf = 0.1 m (see Figure 2b). Fundamental solutions for a quarter space are used to reduce the discretization and to ensure that no spurious transmissions occur through the back of the model.

Figure 3a depicts the results computed by the BEM and MFS when the average spacing between collocation points is 0.005 m and the virtual sources are located at a distance of 0.02 m from the boundary. The displayed results correspond to the normalized acoustic impedance at $x = 0.05$ m, and there is an excellent agreement between the BEM and MFS responses. It should be mentioned that, for the MFS model, the calculation of the impedance is performed as

$$Z(\boldsymbol{x}, k) = \frac{p(\boldsymbol{x}, k)}{v(\boldsymbol{x}, k, \vec{n})} = \frac{\sum_{j=1}^{NS1} Q_j G^{2D}_{sym}(\boldsymbol{x}, \boldsymbol{x}_{1,j}, k)}{\sum_{j=1}^{NS1} Q_j H^{2D}_{sym}(\boldsymbol{x}, \boldsymbol{x}_{1,j}, k, \vec{n})} \quad (27)$$

for each collocation point located at $x = 0.05$ m, and then taking the average value of all collocation points placed in that position. However, it is interesting to note that spurious behaviours can be observed at specific frequencies when a standard BEM model is used. In this situation, a special numerical treatment is necessary applying, for example, the CHIEF method (see [29]). In the present example, the application of this method with just one point greatly attenuated the contribution of the identified spurious eigenfrequencies. Indeed, for the MFS, no such behaviour was identified at any frequency, and thus no special numerical treatment was required for the computed result.

Although a good match between results was registered, it is important to state that the proposed MFS model also performed faster than the single domain BEM model, while still accounting accurately for the presence of the infinite screen. The computational time and the memory requirements of both implementations were measured on the same computer, for different situations and assuming the excitation frequency of 5 kHz; a non-dimensional (relative) CPU time was computed as the ratio between the CPU time of each BEM model and the CPU time of the MFS model. The tested MFS model corresponds to the one described above, while for the BEM model, different lengths of the flange that simulates the infinite screen (Lf in Figure 2b) were tested. Table I describes the results of this test. As can be seen, for the BEM model, increasing the flange size (and thus allowing for a more accurate description of the infinite screen) leads to an increase in both

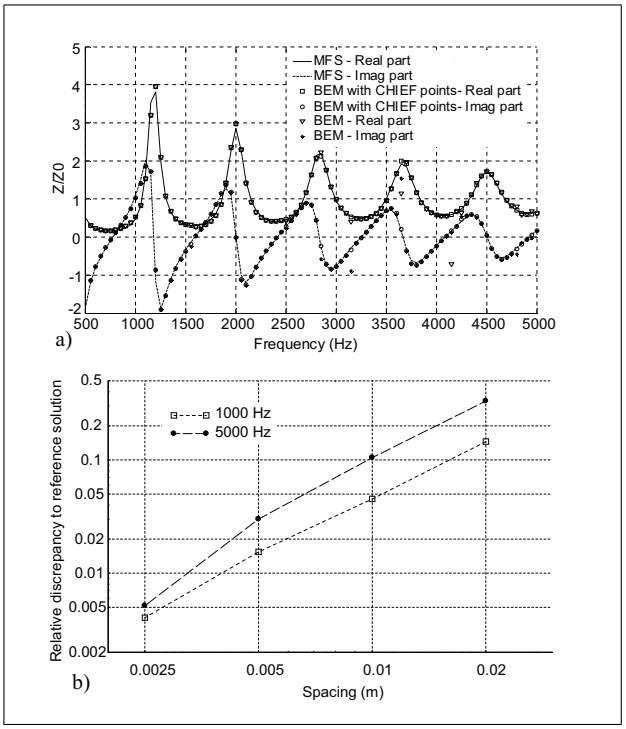


Figure 3. Normalized acoustic impedance calculated for the case of the 2D tube with one vibrating end: a) Results for the BEM (model in Figure 2b) and MFS (model in Figure 2a) when the average spacing between collocation points is 0.005 m and the virtual sources are located at a distance of 0.02 m from the boundary; b) Convergence of the MFS (model in Figure 2a) response for two frequencies when the spacing between boundary points is successively decreased.

the CPU time and the required memory. However, even for the smallest value of Lf (0.1 m), the measured CPU time was almost 20 times that registered for the proposed MFS model; the same occurs in what concerns memory usage, with the proposed model requiring around 8 times less memory than the smallest BEM model tested here.

The convergence of the MFS was analysed for this example using, as a reference for this test, a BEM response computed using an element size of 0.002 m and Lf = 2.0 m (to better reproduce the rigid infinite screen). Results were computed for different average spacings between boundary points, and the average relative discrepancy to the reference solution computed exactly at the horn throat ($|p_{MFS} - p_{BEM}|/|p_{BEM}|$ where $p_{MFS}$ and $p_{BEM}$ are the acoustic pressures computed using the MFS and BEM, respectively) is depicted in Figure 3b for frequencies of 1000 Hz and of 5000 Hz. Indeed, it is clear that the results converge to the reference solution when smaller spacings are adopted, indicating a good behaviour of the method. One should note, however, that the reference solution is also computed numerically, and thus the presented discrepancy is not an exact estimation of the error.

To further scrutinize the MFS model, tests were also conducted for a more refined discretization, with an average spacing between points of 0.0025 m, and considering distances of 0.04 m and 0.005 m between the virtual



*Document downloaded by @DAEL, 2026-05-27 17:11:28 - personal use only*

Table I. Computational performance of the MFS versus BEM models.

| | BEM (1 CHIEF point) | | | | MFS |
|---|---|---|---|---|---|
| | Lf = 1.0 m | Lf = 0.5 m | Lf = 0.3 m | Lf = 0.1 m | |
| Relative CPU time | 71.6 | 37.1 | 26.4 | 17.8 | 1.0 |
| Number of elements or points | 290 | 190 | 150 | 110 | 51 |
| Memory (kB) | 1000 | 564 | 354 | 192 | 22 |

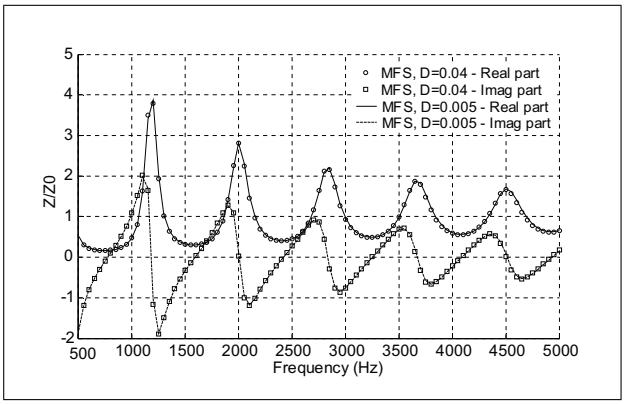


Figure 4. Normalized acoustic impedance calculated for the case of the 2D tube with one vibrating end (see Figure 2a for the geometry) using the MFS with an average spacing between collocation points of 0.0025 m and virtual sources located at a distance D.

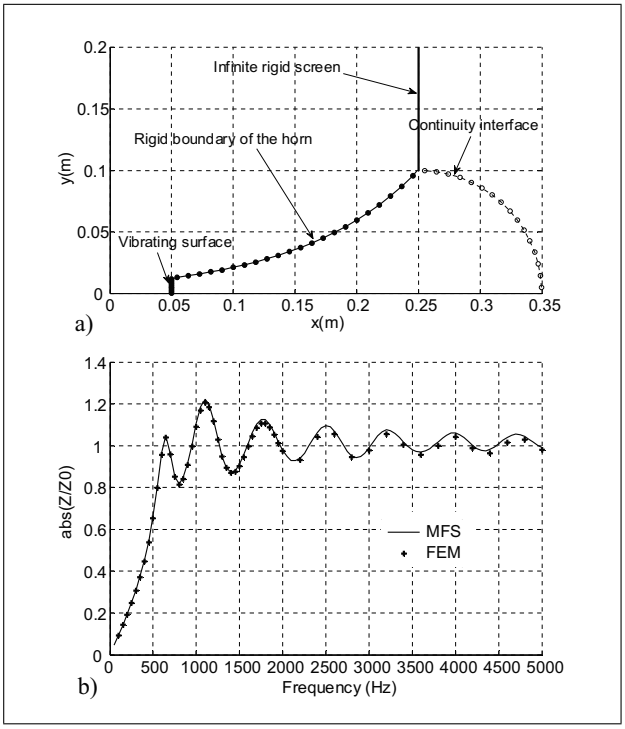


Figure 5. Axisymmetric problem: a) Scheme of the MFS model configuration; b) Computed results in terms of absolute normalized impedance at the horn throat.

sources and the boundary. Figure 4 illustrates the corresponding results and, once again, the computed curves coincide.

It should be mentioned that a suitable choice of the distance of the virtual sources to the contour must be made to obtain reliable accurate results. Indeed, it is known that, for the MFS, if the virtual sources are placed very close to the boundary, the proximity of a singularity of the approximating functions (fundamental solutions) to the boundary of the model tends to lead to unreliable results, and thus very small distances should be avoided.

To verify the accuracy of the MFS when analysing axisymmetric problems, an exponential horn geometry with a throat diameter of 0.0254 m and a mouth diameter of 0.200 m is considered; considering the throat to be positioned at $x = 0.05$ m, the geometry of the horn can be defined as $y = 0.0127\mathrm{e}^{10.3178(x-0.05)}$. The geometry of the corresponding MFS model is depicted in Figure 5a, considering the average spacing between collocation points to be 0.01 m. In Figure 5b the results provided by the MFS model are compared with the results computed using the FEM software, making use of a finite element mesh defined for the upper frequency (5000 Hz), assuming 20 elements per wavelength. To account for the infinite propagation domain, a spherical Perfectly Matched Layer (PML) of order 2 is used in the finite element model. In that figure, absolute impedance values, normalized with respect to the reference impedance of air, computed at the horn throat, are displayed for the two methods. As in the previous case, a very good match between the predictions of both numerical models can be observed, indicating a good behaviour of the MFS model. Although not shown, several tests were performed for more refined point distributions and varying distances between virtual sources and the boundary reveal a good stability of the MFS with respect to those parameters.

## 5. Calculation of horn directivity

To illustrate the practical applicability of the proposed method, the behaviour of two axisymmetric horn geometries is analyzed next. An important parameter with regard to the acoustic behaviour of horns is their directivity, which indicates the decay of the radiated sound level at a certain distance with respect to the incidence angle of sound waves coming from the horn. This parameter is generally measured in an anechoic chamber, simulating free field conditions, and mounting the horn embedded in a rigid flat screen. The model defined here directly accounts for the presence of this screen and for the far field radiation conditions, and so it can be directly used for the evaluation of this parameter.



*Document downloaded by @DAEL, 2026-05-27 17:11:28 - personal use only*

The first tested model corresponds to the exponential horn geometry used in the second verification example of the previous section. For this case, the directivity is calculated by evaluating the sound pressure over a number of receivers distributed in a semi-circular manner, at a distance of 1.0 m from the centre of the horn's mouth (see Figure 6a). The horn directivity was evaluated for frequencies of 500 Hz, 2000 Hz and 8000 Hz, and is displayed in Figure 6b. The presented results reveal that, for all frequencies, a progressive decay of the sound pressure level occurs as the angle at which the receiver is placed increases. For lower frequencies, this decay is small, reaching values around 1 dB for 500 Hz. As the frequency increases, the decay becomes more pronounced, and can reach values as high as 23 dB for the frequency of 8 kHz. It is also interesting to note that the directivity curves are very smooth for the lower frequencies, while higher frequencies exhibit a more pronounced oscillatory behaviour due to their smaller wavelength. To check these results, the same system was modelled using the finite element software. The corresponding results are plotted in Figure 6b. As shown in the verification section, the agreement with the MFS computed results is very good. However, it should be mentioned that, in order to obtain accurate results, the FEM mesh used in this analysis was defined using around 12 elements per wavelength for a frequency of 8 kHz, and thus a very large number of elements and nodes had to be used (around $5 \cdot 10^5$ degrees of freedom); by contrast, for the MFS, a constant number of 92 points uniformly distributed along the boundaries and interfaces of the model was enough to allow very good results to be obtained. For this reason, the MFS model allowed a very fast computation when compared with the corresponding finite element software.

In a second test, the optimized axisymmetric acoustic horn design proposed in the works of Noreland *et al.* [8] and Udawalpola *et al.* [9] was considered. The proposed shape of the horn was obtained numerically by these authors with the aim of having optimal radiation efficiency at frequencies in the range 1.6–9.05 kHz, while satisfying a convexity constraint on the flare. The geometry of this horn is schematically displayed in Figure 7, exhibiting a throat radius of 0.0193 m, a mouth radius of 0.1500 m, and a length of 0.1615 m (note the curvature at the edges of the mouth of the horn).

The horn was modelled using the proposed axisymmetric MFS model, distributing a number of boundary points to discretize its rigid surface. It is worth remarking that the optimized horn exhibits a complex geometry, with significant curvature variations along its boundary, thus requiring a large number of points to correctly define its shape. As in other numerical methods (such as the BEM), the geometry may be defined making use of a fixed number of points per wavelength, allowing to use a smaller number of points for lower frequencies, and a higher number for higher frequencies. However, in some cases, this criterion may not be sufficient to allow a correct definition of the boundary shape. In the present case, due to the continuous

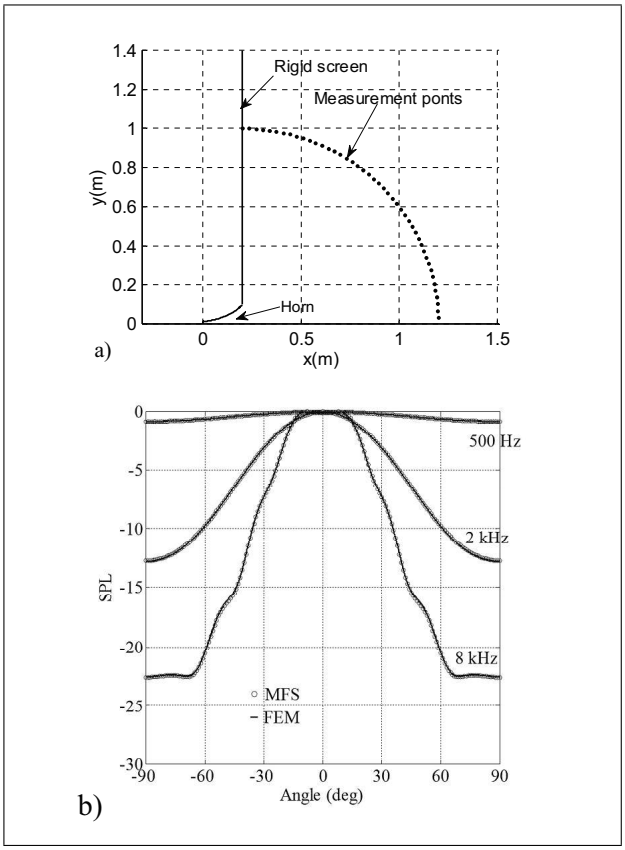


Figure 6. Model of an axisymmetric exponential horn: a) Geometry of the application example; b) Computed directivity results.

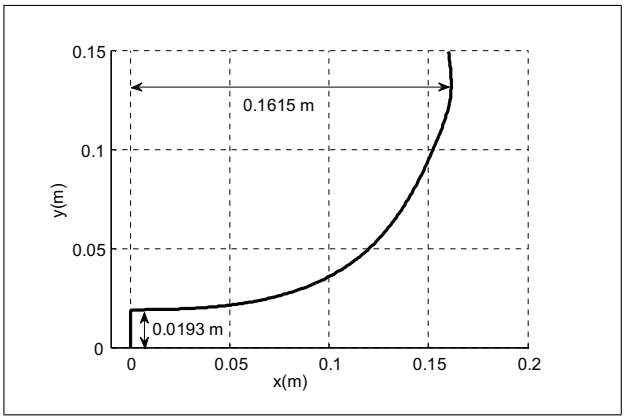


Figure 7. Geometry of the optimized axisymmetric horn proposed by Noreland *et al.* [8].

variation of the horn's curvature, in order to ensure a correct definition of the geometry a total of 113 points were used to build the MFS model for all frequencies, corresponding to approximately 10 boundary points per wavelength for the higher frequency. As in the previous example, beyond the mouth of the horn, an infinite rigid screen is considered and incorporated in the model by means of the virtual sources technique. Figure 8 depicts the directivity results computed for frequencies of 500 Hz, 2000 Hz and 8000 Hz, using both the MFS model and the finite element software. For the latter, and as in the previous case,



*Document downloaded by @DAEL, 2026-05-27 17:11:28 - personal use only*

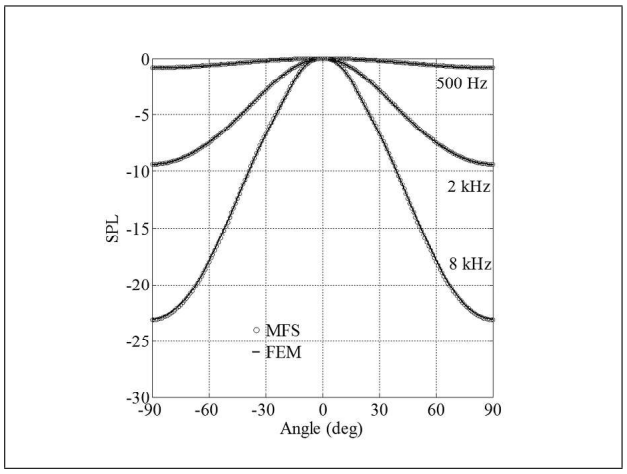


Figure 8. Comparison of directivity results calculated using FEM and using the proposed MFS model, for the geometry represented in Figure 7.

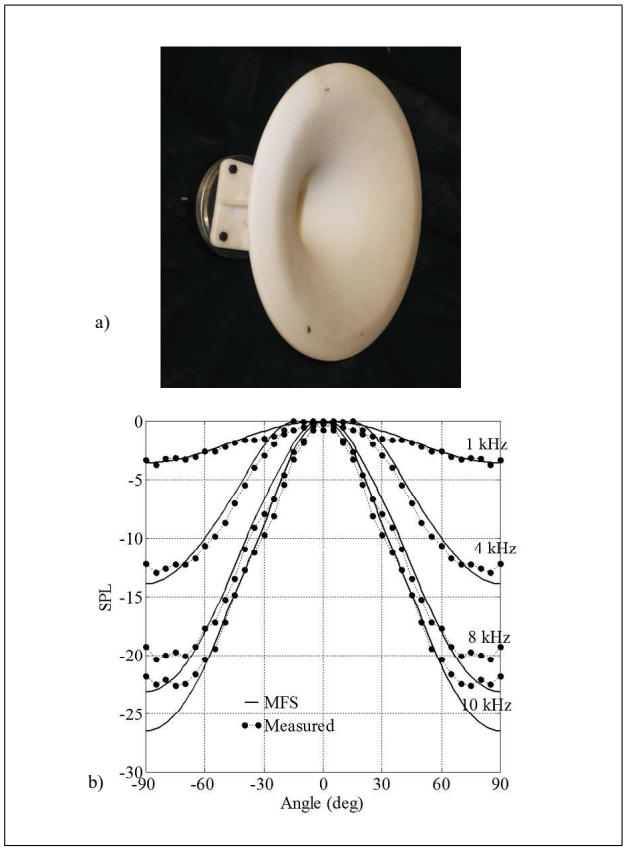


Figure 9. Validation of the numerical model using laboratory measurements: a) horn tested in the laboratory; b) measured and computed directivity results (using the geometry of Figure 7).

the field was discretized making use of a fine mesh, with at least 15 elements per wavelength for a frequency of 8 kHz ($8 \cdot 10^5$ degrees of freedom). As shown in the directivity plots, an excellent agreement exists between both solutions, although with a much lower computational effort in the case of the MFS. It can be noted, in that plot, that the optimized horn exhibits more regular curves, without any observable oscillations along the angular range.

It should be noted that although the two methods have led to very similar results, the calculation performed using the MFS for each frequency was, on average, around 11 times faster than the equivalent calculation using a finite element code; this expressive difference could be even more pronounced taking into account that the finite element package is a highly optimized commercial software, while the MFS implementation was performed in Matlab, and thus it is not an optimized compiled code. Additionally, due to the very small number of points required to define the geometry, the system matrix formed in the MFS led to a RAM memory usage of less than 0.4 MB, while the finite element analysis, requiring a very large number of nodes, led to a memory usage of around 500 MB for the same problem (one should note that since the finite element code used here corresponds to a commercial package, it was not possible to accurately assess the memory used by the application for the calculation itself; so the value presented here was estimated based on the memory usage reported by the operating system during the calculation).

To validate the numerical results shown in Figure 8, the directivity of the horn was measured in laboratory, mounting the horn in a large rigid screen, simulating the theoretical infinite rigid surface of the model. The directivity was measured in anechoic conditions, at a distance of 1m from the mouth of the horn, as described in [30]. In order to obtain the directivity pattern, sound pressure level was registered using a measurement system, and performing sound pressure level evaluations at angular intervals of 5°. In Figure 9a, a photography of the horn tested in the laboratory is depicted. Figure 9b exhibits a comparison of results for frequencies of 1 kHz, 4 kHz, 8 kHz and 10 kHz. The results illustrated in that figure clearly allow concluding that the agreement between numerical results and experimental data is good, although existing some differences between both sets. For the lower frequencies, of 1 kHz and 4 kHz, the trend of the numerical and experimental results is similar, but differences of around 1 dB can be seen even at receivers placed at lower angles. For higher frequencies, a good agreement can be observed for receivers placed at angles up to 60°, without significant deviations between the experimental and numerical results. It is only beyond this angle, for which the decay is over 20 dB, that significant differences (above 1 dB) are registered; these larger differences can be attributed to limitations of the experimental setup used for the directivity measurements.

## 6. Final remarks

In the present paper a numerical model based on the Method of Fundamental Solutions was proposed for the analysis of 2D and axisymmetric acoustic horn systems. The proposed model is based on the use of two sub-regions, one of them containing the rigid horn, and the other corresponding to a semi-infinite space. The joint use of these two sub-regions, connected by imposing the necessary continuity of acoustic pressure and normal particle



Document downloaded by @DAEL, 2026-05-27 17:11:28 - personal use only

velocities, allows simulating the case of an acoustic horn embedded within a rigid screen, a scenario that is frequent in laboratory analysis of such devices.

The model was verified against classic 2D Boundary Element and 3D axisymmetric Finite Element models, and an excellent agreement was found to occur. It must be mentioned that, for the tested cases, the MFS was found to be a very efficient method, requiring only a small number of boundary points to define the proposed horn systems. Indeed, the proposed approach can reduce the required effort both in terms of pre-processing and of computational requirements for the solution of the problems. Indeed, since it doesn't require any discretization of the propagation medium, only the boundaries need to be defined, which is a straightforward task in the model preparation stage; additionally, by only discretizing the boundaries, the final dimension of the problem is much smaller, and thus less demanding from a computational point of view. It is also worth noting that, when compared with the BEM for a 2D problem, the MFS revealed no influence of the well-known spurious eigenfrequencies effect that pollutes the BEM results at some frequencies.

The model was finally applied to study the behaviour of two horn geometries in terms of directivity at different frequencies. For those cases, an excellent agreement with the finite element software was observed. Comparison with experimental results obtained for an optimized non-trivial shape horn also revealed a very good agreement, indicating that the method performs well and can be a valuable analysis tool.

## Acknowledgement

The authors would like to thank the help and support of the company "D.A.S. Audio, S.A.", and particularly of Pablo Seoane, in the preparation of the axisymmetric horn model used in the laboratory tests.

## References

[1] D. Davis, E. Patronis: Sound system engineering. Focal Press, 2006.

[2] G. R. Putland: Every one-parameter acoustic field obeys Webster's horn equation. J. Audio Engineering Soc. **41** (1993) 435–451.

[3] E. Eisner: Complete solutions of the "Webster" horn equation. J. Acoust. Soc. Am. **41** (1967) 1126–1146.

[4] D. B. Keele: What's so sacred about exponential horns? AES preprint 1038, 1975.

[5] S. Morita, N. Kyono, S. Sakay, T. Yamabuchi, Y. Kagawa: Acoustic radiation of a horn loudspeaker by the finite element method. A consideration of the acoustic characteristic of horns. J. Acoust. Soc. Am. **30** (1982) 896–905.

[6] C. Beltran: Calculated response of a compression driver using a coupled field finite element analysis. Presented at the 105th Convention of the Audio Eng. Soc., 1998.

[7] T. Hodgson, R. Underwood: BEM computations of a finite-length acoustic horn and comparison with experiment. The Built Environment **28** (1997) 213–222.

[8] D. Noreland, R. Udawalpola, P. Seoane, E. Wadbro, M. Berggren: An efficient loudspeaker horn designed by numerical optimization: an experimental study. Technical Report UMINF 10.1, Dep. of Computing Science, Umeå University, 901 87 Umeå, Sweden, 2010.

[9] R. Udawalpola, E. Wadbro, M. Berggren: Optimization of a variable mouth acoustic horn. Int. J. Numer. Meth. Engng. **85** (2011) 591–606.

[10] M. Makarski: Tools for the professional developments of loudspeakers. Faculty of Electrical Engineering and Information Technology, Rheinisch-Westfaelische Technische Hochschule Aachen, 2006.

[11] R. C. Morgans: Optimisation techniques for horn loaded loudspeakers. School of Mechanical Engineering, The University of Adelaide, Australia, 2004.

[12] M. Lampton: Transmission matrices in electroacoustics. Acustica **39** (1978) 239–251.

[13] W. P. Patrick: Systematic method to determine the acoustical characteristics of series-parallel duct configurations using transmission matrices. J. Acoust. Soc. Am. **58** (1975) S6–S6.

[14] J. S. McLean, J. T. Post, E. L. Hixson: A theoretical and experimental investigation of the throat impedance characteristics of constant directivity horns. J. Acoust. Soc. Am. **92** (1992) 2509–2520.

[15] S. N. Atluri: The Meshless Method (MLPG) for domain and BIE discretizations. Tech Science Press, 2004.

[16] E. Kansa: Multiquadrics. A scattered data approximation scheme with applications to computational fluid-dynamics. I: Surface approximations and partial derivative estimates. Computers & Mathematics with Applications **19** (1990) 127–145.

[17] h. E. Kansa: Multiquadrics. A scattered data approximation scheme with applications to computational fluid-dynamics. II: Solutions to parabolic, elliptic partial differential equations: Computers & mathematics with applications. 19 **1990** (147-161).

[18] G. Fairweather, A. Karageorghis: The method of fundamental solutions for elliptic boundary value problems. Advances in Computational Mathematics **9** (1998) 69–95.

[19] G. Fairweather, A. Karageorghis, P. A. Martin: The method of fundamental solutions for scattering and radiation problems. Engineering Analysis with Boundary Elements **27** (2003) 759–769.

[20] M. Golberg, C. S. Chen: The method of fundamental solutions for potential, Helmholtz and diffusion problems. Boundary integral methods: Numerical and. Mathematical Aspects Comput. Mech. Publ. **1** (1998) 103–176.

[21] C. Alves, S. Valtchev: Numerical comparison of two meshfree methods for acoustic wave scattering. Engineering Analysis with Boundary Elements **29** (2005) 371–82.

[22] L. Godinho, A. Tadeu, N. Simões: Accuracy of the MFS and BEM on the analysis of acoustic wave propagation and heat conduction problems. Advances in the meshless method. Tech Science Press, 2005.

[23] L. Godinho, A. Tadeu, P. Amado Mendes: Wave propagation around thin structures using the MFS. Computers Materials & Continua **5** (2007) 117–127.

[24] J. António, A. Tadeu, L. Godinho: A three-dimensional acoustics model using the method of fundamental solutions. Engineering Analysis with Boundary Elements **32** (2008) 525–531.



*Document downloaded by @DAEL, 2026-05-27 17:11:28 - personal use only*

[25] L. Godinho, F. G. Branco, P. Amado Mendes: 3D multi-domain MFS analysis of sound pressure level reduction between two enclosures. Archives of Acoustics **36** (2011) 575–601.

[26] V. Pagneux, N. Amir, J. Kergomard: A study of wave propagation in varying crosssection waveguides by modal decomposition. Part I: Theory and validation. J. Acoust. Soc. Am. **100** (1996) 2034–2048.

[27] N. Amir, V. Pagneux, , J. Kergomard: A study of wave propagation in varying cross-section waveguides by modal decomposition. Part II: Results. J. Acoust. Soc. Am. **101** (1997) 2504–2517.

[28] T. Hélie: Unidimensional models of acoustic propagation in axisymmetric waveguides. J. Acoust. Soc. Am. **114** (2003) 2633–2647.

[29] T. Wu: Boundary element acoustics. WIT Press, 2000.

[30] AES2-1984: AES recommended practice. Specification of loudspeaker components used in professional audio and sound reinforcement, 2003.



*Document downloaded by @DAEL, 2026-05-27 17:11:28 - personal use only*